Thin Solid Films 527 (2013) 186–192

Contents lists available at SciVerse ScienceDirect

Thin Solid Films

journal homepage: www.elsevier.com/locate/tsf

Elongation of gold nanoparticles by swift heavy ion irradiation: Surface plasmon resonance shift dependence on the electronic stopping power

C. Harkati Kerboua [a], J.-M. Lamarre [b], M. Chicoine [a], L. Martinu [b], S. Roorda [a,*]

[a] Physics Department, Université de Montréal, CP 6128, succ. Centre-Ville, Montréal, Québec, Canada H3C 3J7
[b] Department of Engineering Physics, École Polytechnique de Montreal, CP 6079, succ. Centre-Ville, Montréal, Québec, Canada H3C 3A7

ARTICLE INFO

Article history:
Received 3 August 2011
Received in revised form 27 October 2012
Accepted 7 December 2012
Available online 19 December 2012

Keywords:
Nanoparticle
Shape transformation
Shift heavy ion irradiation
Surface plasmon resonance
Ion track

ABSTRACT

Gold nanoparticles embedded in a silica matrix were irradiated with 2 to 40 MeV Cu or Si ions at fluences ranging from 1×10^{13} to 4×10^{15} ions/cm^2, and their deformation from spheres to prolate ellipsoids with major axis parallel to the ion beam was studied using *P* and *S* polarized light. For fixed ion energy, the longitudinal surface plasmon resonance (SPR) at 520 nm is red-shifted with an increase of the ion fluence up to a certain value where it reaches a plateau indicating that a maximum aspect ratio is obtained. This saturation in the wavelength shift was found to depend on the ion energy and reaches a maximum of 40 nm. The SPR shift was also used to measure the electronic stopping power dependent deformation rate and to deduce the electronic stopping power threshold of (1.9 ± 1.3) keV/nm required for shape transformation of the embedded gold nanoparticles. Ion track diameters of 0.18 to 1.4 nm were inferred from the fluence dependence of the SPR shift. Analysis by transmission electron microscopy shows that large ($d>10$ nm) particles are more elongated than smaller ones. Our data are consistent with a mechanism of gold nanoparticle elongation requiring both the silica matrix and the nanoparticles to melt following the passage of the swift heavy ion and with elongation being due to the relief of stress in the gold nanoparticle which had built up as a consequence of the deformation of the surrounding silica matrix.

1. Introduction

Ion irradiation produces many effects on condensed matter such as anisotropic deformation at constant volume of single colloidal particles [1,2] and glass foils [3,4], wafer curvature of thin films constrained on substrates [5–7], densification [6] and phase transformation [8]. Among these examples, we investigated previously the spherical gold–silica core–shell colloid system [9]. The silica shells were shown to transform into oblate ellipsoids with its minor axis parallel to the ion beam whereas the gold cores deformed into prolate ellipsoids with its major axis parallel to the ion beam. Simply put, the silica shell shrinks in the direction of the ion beam whereas the gold core elongates. In order to go beyond an incomplete description of this process, we have prepared and investigated Au nanoparticles embedded in silica films [10–12] as it was shown that Au particles deform more efficiently if the surrounding silica shell is thick [9] and not at all when surrounded by a non-deforming crystalline matrix such as AlAs [13]. The mechanism responsible for the deformation of the nanoparticles has not been uniquely identified, but it appears that both anisotropic deformation of the surrounding matrix [1,9,14,15] and melting of the nanoparticle play an essential role [15–18]. The electronic, magnetic, and optical properties of metallic nanoparticles embedded in a dielectric matrix are very interesting and depend strongly on the nanoparticle size, shape, orientation, interparticle distance, and environment [10,12]. The fabrication, modification, and characterization of these heterogeneous nanocomposite materials is an active field of research motivated by the potential applications in optical and optoelectronic devices [19,20], biosensing [21], and in medical applications [22].

When ions are slowed down in condensed matter they deposit a vast amount of energy within a small material volume, during a short time. This energy is lost via two distinct mechanisms: i) elastically by scattering of the projectile on the target nuclei, and ii) inelastically by ionization and electronic excitation of target atoms [3,23]. Both mechanisms strongly depend on the kinetic energy of the incident ion. For high energy heavy ions, electronic interactions dominate and the ion loses energy at a rate of a few to a few tens of keV per nm. During a short period of time, the system within a small localized region around the ion trajectory is far from equilibrium due to a high density of highly excited electrons. These electrons are initially accelerated towards the center of the ion track and will either undergo scattering or overshoot the track center and end up moving outward while an energy transfer to the atomic network takes place. This energy transfer was explained by two models: the thermal spike model [24–26] and the ion spike model, also known as Coulomb explosion [27,28]. In the first model, the energy is thermalized by electron–phonon coupling and leads to the increase of local temperature. In the second one, kinetic energy of electrons allows them to move far from the ion track leaving behind a cylinder of positively charged ions. The mutual electric repulsive forces between the positive ions lead to ionic Coulomb explosion. Hybrid

* Corresponding author. Tel.: +1 514 343 2076; fax: +1 514 343 7357.
E-mail address: sjoerd.roorda@umontreal.ca (S. Roorda).

0040-6090/$ – see front matter
http://dx.doi.org/10.1016/j.tsf.2012.12.007

models have also been proposed [29,30] and validated by simulations [31].

The deposited energy during ion irradiation can affect the crystalline structure, the morphology and other properties of irradiated materials. In particular, amorphous targets can suffer macroscopic deformation, known as anisotropic growth or ion hammering, whereby a thin film becomes thinner and wider upon ion irradiation. This plastic deformation process has been described by a viscoelastic model [32,33] and a hammering model [34,35]. In the first model, the phenomenon is attributed to energy loss and it occurs efficiently at high electronic stopping powers. For intense electronic excitations a cylindrical region around the ion trajectory is heated and the shear stresses induced by the thermal dilatation are relaxed. The residual strains freeze-in upon cooling down. In the second one, a computer simulation of relaxation of mechanically polarized material is used to estimate the plastic flow. The viscoelastic model and ion hammering explain the deformation of amorphous colloids but not the resistance to deformation of crystalline ones. Other models were also proposed to explain material plastic deformation like: Ostwald ripening and creep deformation [36], and generation–relaxation of stress [6].

The viscoelastic model does not explain the deformation of core–shell colloids or nanoparticles embedded in an amorphous planar matrix. However, from the earliest observation of nanoparticle deformation it has been surmised that the visco-elastic response of the matrix plays an important role [1,9,14,15] and thermal spike models involving melting of the nanoparticle have been invoked as well [15–18]. In the current paper, we present experimental results that shed more light on possible physical deformation mechanisms of gold nanoparticles embedded in a silica matrix. We will show by modeling the SPR spectral position that the anisotropic deformation induced by ion irradiation can be controlled by the fluence, the energy and the nature of the ion beam. We will focus our attention on the role of the electronic stopping power in the modification of the optical and structural properties of gold/dielectric nanocomposite films.

2. Experimental methodology

Gold/silica nanocomposite films were deposited on fused silica substrates by simultaneous sputtering of a pure gold target and plasma-enhanced chemical vapor deposition of SiO_2 using a SiH_4–O_2 gas chemistry. High temperature (900 °C) annealing in ambient atmosphere for 9 h was used in order to increase the size of gold particles. These two preparation steps were studied and described in detail earlier [10].

A series of identical samples (~200 nm thick and 1.8 at.% gold concentration) were irradiated with 2 to 40 MeV Si and Cu ions accelerated using Tandem or Tandetron accelerators. During the ion implantation, the samples were mounted on a liquid nitrogen-cooled copper block but on a few occasions the samples were irradiated at room temperature. Irradiating at liquid nitrogen temperature may lead to slightly faster quenching rates, and to more efficient freezing-in of metastable features. All samples were implanted at 45° off the surface normal. The ion beam was electrostatically scanned to uniformly irradiate several areas (0.5×1.5 cm^2) of the same sample. The base pressure during ion irradiation was 1×10^{-6} Torr (1.33×10^{-4} Pa). The ion beam fluence ranged from 1×10^{13} to 4×10^{15} ions/cm^2. The beam flux was maintained between 6×10^{10} and 8×10^{11} ions/(cm^2.s). The initial charge state of ions varied from Si^+ to Si^{7+} and from Cu^{2+} to Cu^{7+}. The SRIM code [37] was used to calculate the projected ranges R, the electronic and nuclear energy losses in silica for different irradiating ions (Si and Cu), and energies (2 to 40 MeV). We assumed a SiO_2 density equal to 2.32 g/cm^3. The results confirm that the projected ranges are much larger than the Au/SiO_2 film thicknesses for all used energies. This means that most of the ions will end their trajectory in the substrate region, after irradiating the nanocomposite throughout its thickness. For each energy value, the electronic energy loss is considerably greater than the nuclear energy loss. Therefore, most of the engendered morphological and structural modifications in irradiated nanocomposite samples will result from electronic interactions.

The optical response and microstructural properties of gold nanoparticles before and after irradiation were investigated. Polarized transmission measurements were performed on a variable angle spectroscopic ellipsometer (J.A. Woollam). Transmission electron microscopy (TEM) observations were carried out using a JEOL JEM 2100F transmission electron microscope operating at 200 kV and equipped with a Gatan imaging filter and scanning (STEM) mode. The examined specimens were prepared in cross-sectional orientation using a conventional technique for mechanical polishing and ion thinning. The ion thinning was performed using a Precision Ion Polishing System.

3. Results and discussion

3.1. Size/shape versus fluence correlation

Fig. 1 shows cross-section TEM pictures of Au/SiO_2 nanocomposite films after irradiation with 8 MeV Cu^{+3} ions at two fluences: 2.5×10^{14} and 1.5×10^{15} ions/cm^2. One can see that spherical and ellipsoidal gold particles are present in both irradiated samples. The deformation is more marked in the high fluence case (Fig. 1b). The long axes of the ellipsoidal nanoparticles are aligned with the direction of the ion beam, indicated by an arrow in each of the two panels. We have measured the long (c) and short (a) axes of each ellipsoidal gold nanoparticle and calculated an effective particle diameter ($2r_{eff}$) corresponding to the diameter of a sphere of same volume ($^3/_4\pi a^2 c = {}^3/_4\pi r_{eff}^3$). The aspect ratio ($c/a$) was evaluated and plotted versus $2r_{eff}$ before and after irradiation with 8 MeV Cu ions in Fig. 2. In non-irradiated samples, all gold particles are spherical and their size does not exceed 14 nm. After irradiation the shape of the majority of the metallic particles changes from spherical to ellipsoidal ($c/a \neq 1$) with different aspect ratios. The maximum aspect ratio and effective particle size observed at a fluence of 2.5×10^{14} ions/cm^2 are smaller than those obtained for 1.51×10^{15} ions/cm^2. Fig. 2 also shows that the most elongated particles are those which have the largest effective size and that most of those which remain spherical are small, and that no particles smaller than 4 nm deform. Other reports found that particles smaller than 5 and larger than 50 nm don't deform [16] or that a deformation threshold of 7 nm exists [18], but in both of those studies, samples were presumably irradiated at room temperature. The volume of the majority of particles increases with ion fluence, which was of course not observed in our earlier experiments involving core–shell colloidal particles [9] but has been observed by other distributed-size systems [38]. Thus, the elongation of gold particles is not exclusively caused by a direct transformation as in the case of colloids. Since only two ion fluences were studied by TEM, the behavior at higher fluences will be investigated below, using optical characterization. At least one of three other phenomena seems to occur during ion irradiation: coalescence, Ostwald ripening, or growth from Au atoms still in solution. Indeed, when STEM pictures taken before and after irradiation at high magnification were analyzed (not shown here), very small gold clusters with size lower than 1 nm were observed in irradiated samples but were not present in non-irradiated ones. These could be pre-existing particles that have almost dissolved (Ostwald ripening) or newly formed particles from Au atoms still in the solution.

We have also observed coalescence processes, that is, when gold particles are in contact they merge together forming one larger and longer particle. Coalescence process reduces the surface in order to minimize the energy. Fig. 3 illustrates two examples of gold particle elongation by coalescence with a preferential direction due to the ion beam, both at liquid nitrogen (Fig. 3a) and room temperature (Fig. 3b). Fig. 3b presents a high resolution TEM picture of a sample irradiated at room temperature with 30 MeV Cu^{+5} at a fluence of 1×10^{15} ions/cm^2. One can observe the presence of gold atomic

planes and columns in two ellipsoidal particles which appear to be regrouping towards one nanorod. Neither image shows clear evidence of faceting such as has been observed in larger particles irradiated under conditions of much higher electronic energy loss [38]. The simple observation of a particle that appears to have been formed by coalescence cannot by itself rule out that the particle was formed by a combination of deformation and growth from adsorption of Au in solution. However several other facts should be considered: in the case of deformation of colloidal Au particles embedded in silica [15] (distinct from the particles in our case made by thermal treatment of an atomic Au dispersion as opposed to inclusion of pre-fabricated colloidal particles) coalescence was also observed; we observed (Fig. 2) an increase in the largest observed particle size following irradiation. Thus we conclude that the particles seen in Fig. 3 most likely result from deformation and coalescence.

3.2. SPR position dependence on fluence and electronic energy loss

The optical properties of our metal/dielectric nanocomposites depend on the shape and alignment direction of the gold particles. The SPR position can be controlled using ion beam irradiation [10,11] and the SPR shift was observed to saturate at high fluences but no detailed explanations on the mechanism were given at the time. To better understand this phenomenon, optical measurements were carried out using light with a propagation direction perpendicular to the ion beam direction. In this geometry, polarized light can excite one of the two SPR modes: the transversal mode perpendicular to the ion beam for *S* polarization, or the longitudinal one parallel to it for *P* polarization (for the measurement geometry, see Fig. 1 of reference [11]). Of course, for spherical particles, *P* and *S* polarized transmission spectra are identical with only one SPR at 518 nm since the longitudinal and transversal modes are degenerate. This value corresponds to the surface plasmon dipole excitation of isolated gold nanoparticle in a silica matrix. Fig. 4 presents *P* and *S* transmission spectra for the sample irradiated with 8 MeV Si ions at various fluences. One can see that the position of the transversal SPR shifts to higher energies while the position of the longitudinal SPR shifts towards lower energies with the increase of the ion fluence. This SPR behavior corresponds to an increase of gold particle dimension parallel to the ion beam (long *c*-axis) and a dimension decrease perpendicular to it (short *a*-axis).

In order to further study the SPR shift, we performed a set of measurements similar to those presented in Fig. 4 but with two different kinds of ions (Si and Cu) and with energies ranging between 2 and 40 MeV. Under these conditions, the maximum SPR shift (from 518 nm for spherical particles) was up to 560 nm for the longitudinal mode and 495 nm for the transverse mode. Note that the shift of the longitudinal mode is larger than that of the transverse one. We calculated the normalized SPR wavelength shift Δλ, for *P*-polarized transmission measurements and plotted it in Fig. 5 against the fluence. At fixed ion energy, Δλ shows a rapid increase with the ion fluence and then reaches a plateau indicating that a maximum particle aspect ratio have been obtained. The saturation indicates that subsequent ions irradiating the nanocomposite do not create notable additional structural changes. This can be described using a simple track-overlap model corresponding to the following expression [39,40]:

$$\Delta\lambda = \Delta\lambda_0\left(1 - Me^{-F/F_0}\right). \quad (1)$$

In this equation, $\Delta\lambda_0$ is the maximum SPR wavelength shift at saturation and *M* is a fit parameter depending on the geometry of the

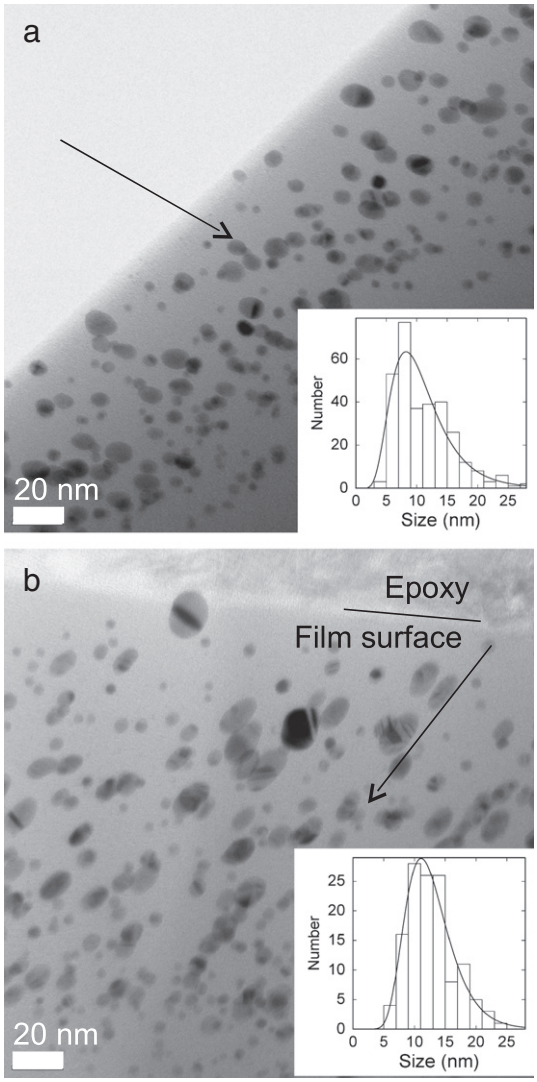

Fig. 1. Cross-sectional TEM images of gold nanoparticles embedded in silica after irradiation with 8 MeV Cu ions to a fluence of 2.5×10^{14} ions/cm^2 (panel a) and 1.51×10^{15} ions/cm^2 (panel b). The arrows indicate the direction of the incident ion beam. The inset shows the size distribution of the gold particles, where the size is expressed as an effective radius (see text).

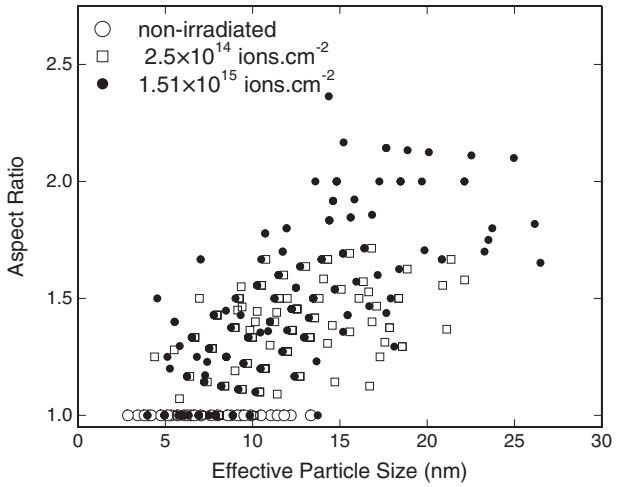

Fig. 2. Measured aspect ratio of gold nanoparticles, plotted versus the size of the particle. For non-spherical particles, the effective size is calculated as explained in the text. Open circles correspond to non-irradiated particles, open squares to particles irradiated with 2.5×10^{14} ions/cm^2, and solid circles to particles irradiated with 1.51×10^{15} ions/cm^2.

experiment and the material, F is the fluence and F_0 is the characteristic fluence. The solid lines in Fig. 5 correspond to fits of Eq. (1) to each of the corresponding data sets, and the dashed portions indicate extrapolation of Eq. (1) with the resulting fitting parameters. These fits show that the SPR shift as a function of ion fluence is well described by such a simple track-overlap model. The saturation levels in the case of Cu ions are higher than those observed in the case of Si. This shows that the saturation in the shift is indeed related to the saturation in the shape deformation of the particles, and not to saturation in the optical response itself. In the case of Cu ions, saturation is reached for relatively small fluences compared with those required in the case of Si. Both these observations can be correlated with the electronic stopping power value which is higher for Cu ions than for Si ions even for the same energy. Indeed, for higher electronic stopping power, more energy per ion is transferred to the material. This leads to a more efficient deformation per ion (faster saturation) and a greater potential for deformation (larger shift). Although these trends are borne out by the majority of the data, a few points corresponding to irradiation at 40 MeV appear anomalous. We speculate that perhaps, in the case of irradiation with 40 MeV Si ions, heat sinking of the samples to the liquid-nitrogen cooled sample holder was only partly successful, or that perhaps an error occurred in accurately measuring the current caused by the multiply charged ions incident on the insulating substrates.

Fig. 6 presents the dependence of $\Delta\lambda_0$ on the electronic stopping power; it shows that the maximum SPR shift stays constant at high electronic stopping power indicating again that the energy transfer is sufficient for maximum deformation. The trend of the data also shows that a minimum electronic stopping power of (1.9 ± 1.3) keV/nm is necessary to produce a SPR shift. We have also calculated the initial SPR shift rate, Γ, which is defined as the slope of the expression presented in Eq. (1) for small fluences. This corresponds to:

$$\Gamma = \frac{d(\Delta\lambda)}{dF} = \frac{\Delta\lambda_0 M}{F_0} e^{-F/F_0} \approx \frac{\Delta\lambda_0 M}{F_0} \text{ for } F \ll F_0. \quad (2)$$

Γ is plotted against the electronic stopping power for different irradiating ions (Cu and Si) in Fig. 7. After an effective threshold at (1.9 ± 1.3) keV/nm (see also Fig. 6), the shift rate increases slightly with the electronic stopping power up to 4 keV/nm. At this value the shift rate rises abruptly and remains high even if the electronic stopping power of the ions is increased. This electronic stopping power threshold for deformation of gold particles by silica matrix is very close to the value of (2.0 ± 0.5) keV/nm measured by others [4] and somewhat lower than the value of ~3.3 keV/nm found in core–shell colloidal particles [1]. Such differences in threshold may be

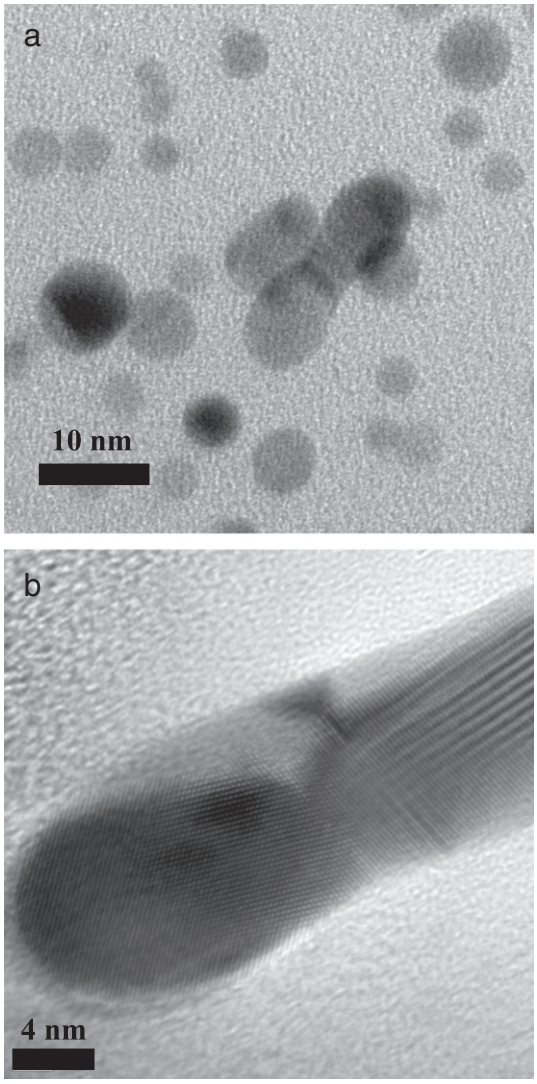

Fig. 3. TEM images showing elongated gold particles in a sample irradiated: a) at liquid nitrogen temperature with 8 MeV Cu ions to a fluence of 1.51×10^{15} ions/cm^2, and b) at room temperature with 30 MeV Cu ions to a fluence of 1.00×10^{15} ions/cm^2.

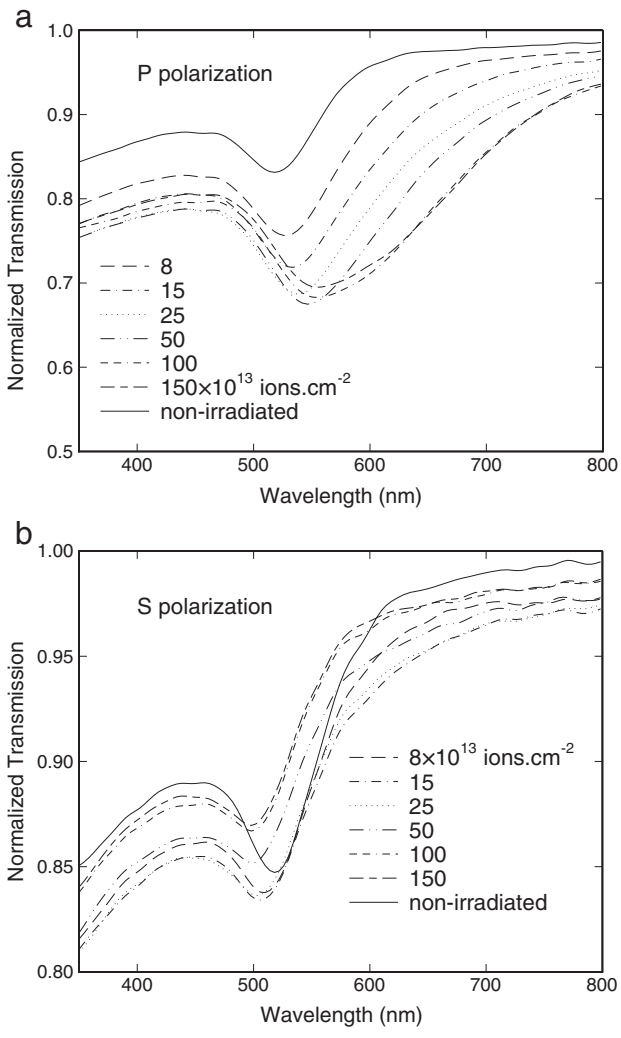

Fig. 4. Optical transmission in P (panel a) and S (panel b) polarization for samples irradiated with 8 MeV Si ions at different fluences. The SPR position is shifted to longer (P) or shorter (S) wavelengths as a result of the increasing particle aspect ratio with the fluence.

due to a difference in target temperature during the irradiation; using liquid nitrogen cooling leads to somewhat faster quenching rates and is likely more efficient at freezing in un- and meta-stable structures.

The estimation of the inferred diameter (d) of the ion track is possible from the F_0 value because F_0 corresponds to the fluence where a fraction of exactly $1/e$ of the total surface S_{tot} remains untouched by ions. The irradiated area S_{irr} is given by the expression:

$$S_{irr} = S_{tot}\left(1 - \exp\left(-\frac{S_i}{S_{tot}}n\right)\right) \quad (3)$$

where S_{tot} is the surface exposed to the ion beam, S_i is the surface area of an isolated ion impact site, and n is the number of ions which arrives on the surface exposed to the ion beam.

Knowing that $S_{tot} = \pi\left(\frac{d}{2}\right)^2$, one can thus write:

$$d = 2\sqrt{\frac{1}{\pi F_0}}. \quad (4)$$

The inferred track diameter is plotted as a function of the electronic stopping power in Fig. 8. As was the case with the SPR shift rate, the inferred diameter shows a threshold near 2 keV/nm and appears to saturate at higher stopping powers. In the same figure and its inset, we compare our results with other measurements and estimates available in the literature, namely with recent, direct measurements of the total and core radius by small angle x-ray scattering (SAXS) [41] and with older measurements deduced from the fluence dependence of the saturation of the IR absorption at 1078 cm^{-1} [42].

As can be seen in the inset, which depicts the data on a scale of 0–10 nm, the diameters inferred from the plasmon shift are much smaller than the total diameter measured by SAXS and the diameter inferred from IR absorption saturation. It is also clear, from the main figure, that the inferred diameter corresponds to that of the track's core as measured by SAXS [41]. Interestingly, the IR results are deduced from a track-overlap argument similar to the one we used in our present analysis. The different results (i.e., IR agrees with *total* radius from SAXS, whereas our results agree with *core* radius from SAXS) are not due to the mathematical model describing the fluence dependence but are more likely a consequence of the physics involved: the IR absorption is sensitive to defects in the silica and is expected to correspond to the total track radius; the final size of metal nanoparticle is apparently controlled by the core of the ion track.

The diameters inferred from our all-optical measurements are also comparable to recent results obtained by TEM [43] (not shown in the figure). Both our results and the TEM values are much smaller than estimates deduced from HF etching of latent tracks in silica [44].

3.3. Discussion on the deformation mechanisms

The following scenario for the deformation of silica-embedded gold nanoparticles by shift heavy ion irradiation appears appropriate. (1) Each incoming ion melts (very briefly) a narrow silica cylinder (the latent track) and (2) the cumulative effect of many separate ion impacts is the anisotropic growth (flattening and widening) of the silica matrix. (3) This deformation puts in-plane compressive stress on the gold nanoparticles, which can be relieved by elongating in the direction of the ion beam. (4) This happens when a swift heavy ion traverses a gold nanoparticles and melts it, again only along the ion track and only very briefly. In other words, radial material fluxes in the hot cylindrical region around the ion tracks created in silica act like a “hammer and anvil” on gold NPs which deform to accommodate cumulative stresses induced by each ion in the surrounding matrix. After the passage of the ions, the strain in amorphous silica “freezes” upon cooling down of the spike region whereas gold nanoparticles recrystallize. The first three stages of this simple scenario were recognized early on [9] whereas the need for the nanoparticle to melt was suggested [36] and later found to be required [35]; the 4-step scenario is consistent with

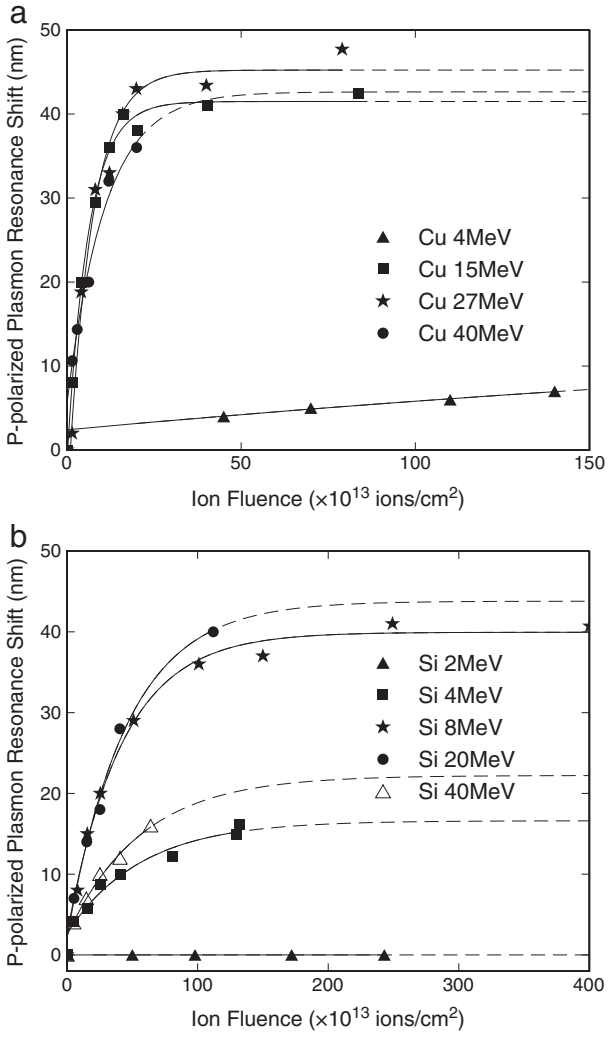

Fig. 5. Shift of the longitudinal SPR band measured in *P* polarization as a function of the ion fluence for different beam energies (panel a: Cu ions and panel b: Si ions). The symbols represent the experimental data and the solid lines are the theoretical fits using the ion track overlap model discussed in the text.

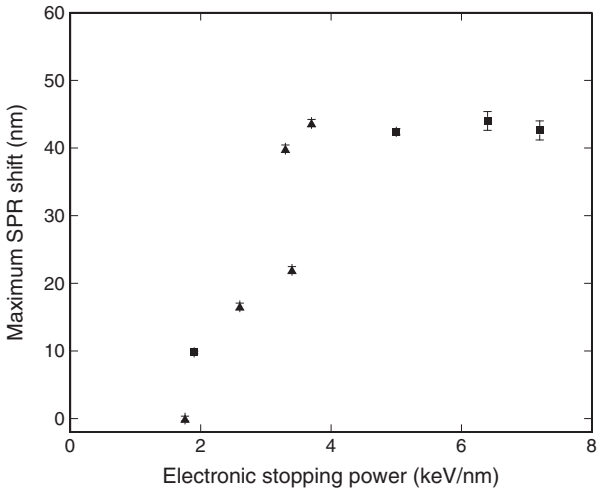

Fig. 6. Maximum SPR wavelength shift plotted against the electronic stopping power for Cu (■) and Si (▲) ions. The data are extracted from Fig. 5.

all old and new experimental data. We note a recent result that a *non-overlapping ion* impact can deform Zn nanoparticles embedded in a silica matrix [45]; even at the low fluences studied in [45], a significant number of ion impacts have also occurred on the surrounding matrix so this work does not exclude steps (2) and (3) in our scenario. Depending on the preparation method of the nanocomposite, differences in thermal expansion coefficients may lead to an initial stress on the nanoparticle being present even before the irradiation begins, which is then relieved as soon as ions impact a nanoparticle.

Our present measurements demonstrate the existence of a threshold electronic stopping power value needed for the deformation of gold nanoparticles. This threshold is close to that for deformation of silica, believed to be related to melting along the ion track. Moreover, the fact that isolated (without a surrounding dielectric matrix) spherical gold particles irradiated with heavy energetic ions present no deformation [9,46] supports the idea that the silica matrix plays a crucial role in the deformation.

Stages (3) and (4) of our scenario require some special attention. Calculations have shown that the threshold for melting of the silica matrix is close to the threshold for melting of the Au particle itself [16], therefore it becomes difficult to positively identify the need for melting of the gold nanoparticle. However, the deformation of the silica around the ion trajectory is accompanied by generation and relaxation of stress. Brongersma et al. [6] showed that in-plane tensile stresses are generated in silica films during swift heavy ion irradiation. Their magnitude is about 150 MPa for fluences around 2×10^{13} ions/cm^2, much less than the yield strength of solid gold. However, the enhanced mobility of gold atoms in the liquid phase would readily explain the formation of ellipsoidal NPs. Recently, a 3-D calculation of heat flow in and around a gold nanoparticle embedded in silica following the impact of a swift heavy ion has been reported [47]. Even though these calculations concern an ion impact (110 MeV Br) and nanoparticle (20–40 nm) quite different from the parameters used in our study, these calculations found that the gold particle can be melted, sometimes partially, even when the ion impact is not directly on the particle but in its close proximity. The 4-step scenario appears consistent with these calculations.

One aspect of the deformation of gold nanoparticles appears anomalous at first sight: the anisotropic elongation of gold nanoparticles *saturates* at high fluences whereas silica thin films show *unsaturable* plastic flow in the direction perpendicular to the ion beam [32]. The saturation level of SPR shift is observed to depend on deposited energy. When the electronic stopping power is increased, the SPR shift is moved towards higher values, which shows that the saturation in optical response is indeed related to the shape and size of gold nanoparticles and not to the matrix deformation. We speculate, and in fact it is to be expected, that for small radii a competition occurs between surface tension of gold nanoparticles in the brief liquid phase and the compressive stress applied by silica matrix [11]. This competition would have two consequences: smaller particles suffer less deformation than larger particles (as observed, compare Fig. 2), and upon elongation, even large particles attain a small enough radius (short axis) so that surface tension limits further elongation, in other words the deformation saturates, as observed.

We have shown that coalescence and possible Ostwald ripening processes and growth due to the Au atoms in solution in the matrix, which can contribute to NPs elongation, are more pronounced at high fluences (Fig. 2). In conventional heat treatments [10], an extended annealing time does not affect the equilibrium state reached by Ostwald ripening and coalescence. So, when the saturation (stationary equilibrium state) is reached in the irradiated nanocomposite, we can assume that the additional incoming ions depositing energy leads to negligible structural change.

The ion track diameter, corresponding to the momentarily liquefied cylinder in silica or in gold, is smaller than the particle mean size. This means that if some ions cross a gold particle, therefore transferring part of their energy for melting gold, other ions need to have crossed a neighboring silica region to provide the stress required for the deformation. Thus, nanoparticles of the nanocomposite are deformed by the *cumulative* effects of incident ions. However, the absence of incubation fluence (cf. Fig. 5) indicates that relatively few ion impacts are enough to build up sufficient stress leading to deformation and that perhaps some stresses resulting from the sample preparation are present even before the irradiation with swift heavy ions.

The previous models [32–36] for plastic deformation of materials do not treat the morphology transformation of metallic nanoparticles in the nanocomposite Au/SiO_2 system. Based on our experimental studies, we have proposed a mechanism for the deformation of gold NPs embedded in a dielectric matrix. This scenario is consistent with our experimental data and it would be interesting to extend

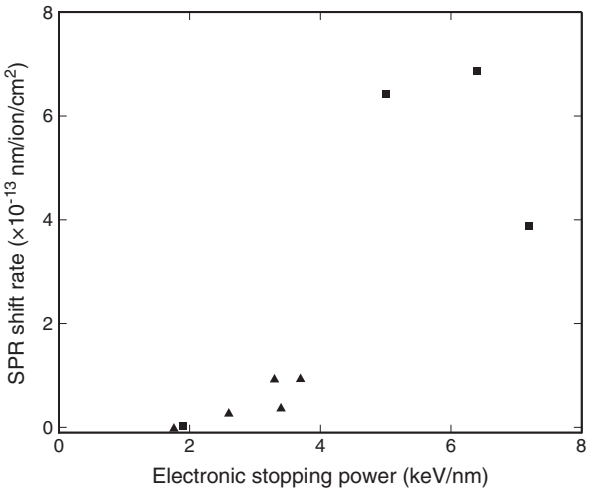

Fig. 7. Gold particle SPR shift rate variation plotted against the electronic stopping power for Cu (■) and Si (▲) ions. The data are extracted from the fit results of Fig. 5.

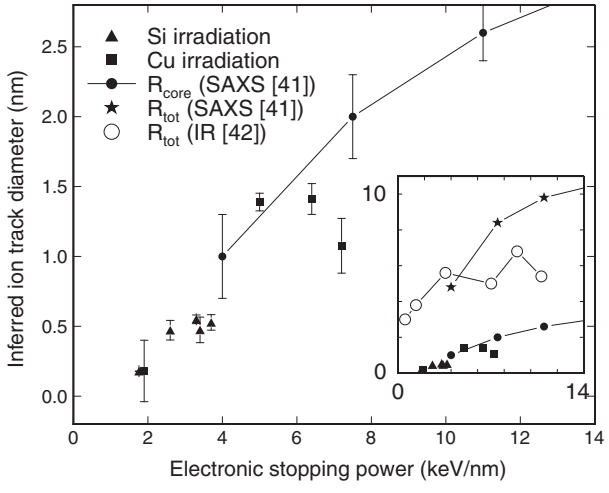

Fig. 8. Inferred ion track diameter as a function of the electronic stopping power. The symbols ▲ and ■ correspond, respectively, to Si and Cu ions. The data are calculated from the fit results of Fig. 5 and Eq. (4). Also shown are the core and total track diameter in silica deduced from small angle x-ray scattering, as reported in ref. [41], and the radius inferred from the saturation of the infrared absorption, as reported in ref. [42]. The main figure shows data up to 2 nm track diameters, larger diameters are shown in the inset.

the existing anisotropic deformation models for the nanocomposite case.

4. Conclusion

High energy ion irradiation on nanometer-size gold nanoparticles embedded nanocomposite in silica was studied. TEM results and polarized transmission measurements confirm that spherical gold nanoparticles are transformed into prolate ellipsoids by swift heavy ion irradiation. The elongation of gold particles embedded in silica is produced by at least two distinct mechanisms: direct deformation by stress from the surrounding amorphous matrix which itself is subject to ion hammering, and coalescence. Statistical analysis of TEM pictures indicates that the average size of the particles increases due to coalescence, although contributions from Ostwald ripening and continued growth from gold still in solution cannot be excluded. As well, large gold nanoparticles are more elongated than small ones which indicates that for small radii, the ion induced deformation competes with surface tension effects. Optical measurements revealed a splitting of the SPR band at 520 nm caused by the irradiation. More specifically, we observed a blue shift by at most 20 nm of the short-axis SPR and a red shift, up to 40 nm, of the long-axis SPR with the increase of the ion fluence. These shifts indicate that the nanoparticle mean aspect ratio increases. A detailed analysis of the SPR position as a function of the ion fluence was described by a simple track-overlap model; analyzing the fit parameters as a function of ion species and energy revealed that the electronic stopping power is the critical parameter governing the deformation. Large SPR shifts, a fast initial deformation rate, and a large saturation value are obtained for ions with high electronic stopping power. In the case of low electronic stopping power ions, the fluences needed for deformation are relatively high. The SPR shift exhibits a threshold value of (1.9 ± 1.3) keV/nm required for deformation. This threshold is the same as that for the deformation of silica, and likely related to the threshold for melting of the silica along the ion track. Above 4 keV/nm, the maximum SPR shift becomes independent of the electronic stopping power. The dependence of the SPR shift on ion fluence can be modeled considering the probability that subsequent ion tracks overlap, and these considerations lead to estimates of the ion track diameter. We find diameters from 0.17 to 1.4 nm, comparable to the diameter of the core of ion tracks in silica as measured by SAXS [41]. All these data appear consistent with a mechanism of deformation whereby the ion irradiation first deforms the silica, which exerts a compressive stress on the nanoparticles in a plane perpendicular to the ion beam, which can be relieved when an ion passes through a nanoparticle and melts it along the ion track. By cumulative impacts, the particle then deforms until the short axis is so small that surface tension becomes too important to allow further deformation.

Acknowledgments

The authors wish to thank Louis Godbout and Réal Gosselin for expert technical support and Jean-Philippe Masse of CM^2 of École Polytechnique de Montréal for his help with the TEM analysis. This work was supported by NSERC of Canada, VRQ (Nanoquébec) and FQRNT (RQMP) of Quebec.

References

[1] J.J. Penninkhof, T. van Dillen, S. Roorda, C. Graf, A. van Blaaderen, A.M. Vredenberg, A. Polman, Nucl. Instrum. Methods B 242 (2006) 523.
[2] T. van Dillen, A. Polman, W. Fukarek, A. van Blaaderen, Appl. Phys. Lett. 78 (2001) 910.
[3] M.-D. Hou, S. Klaumünzer, G. Schumacher, Phys. Rev. B 41 (1990) 1144.
[4] A. Benyagoub, S. Löffler, M. Rammensee, S. Klaumünzer, G. Saemann-Ischenko, Nucl. Instrum. Methods B 65 (1992) 228.
[5] E. Snoeks, A. Polman, C.A. Volkert, Appl. Phys. Lett. 65 (1994) 2487.
[6] M.L. Brongersma, E. Snoeks, T. van Dillen, A. Polman, J. Appl. Phys. 88 (2000) 59.
[7] E. Snoeks, T. Weber, A. Cacciato, A. Polman, J. Appl. Phys. 78 (1995) 4723.
[8] A. Benyagoub, Nucl. Instrum. Methods B 206 (2003) 132.
[9] S. Roorda, T. van Dillen, A. Polman, C. Graf, A. van Blaaderen, B.J. Kooi, Adv. Mater. 16 (2004) 235.
[10] J.-M. Lamarre, Z. Yu, C. Harkati, S. Roorda, L. Martinu, Thin Solid Films 479 (2005) 232.
[11] C. Harkati Kerboua, J.-M. Lamarre, L. Martinu, S. Roorda, Nucl. Instrum. Methods B 257 (2007) 42.
[12] J.-M. Lamarre, F. Billard, C. Harkati Kerboua, M. Lequime, S. Roorda, L. Martinu, Opt. Commun. 281 (2008) 331.
[13] C. Harkati Kerboua, M. Chicoine, S. Roorda, Nucl. Instrum. Methods B 269 (2011) 2006.
[14] Y.K. Mishra, F. Singh, D.K. Avasthi, J.C. Pivin, D. Malinkovska, E. Pippel, Appl. Phys. Lett. 91 (2007) 063103.
[15] E.A. Dawi, G. Rizza, M.P. Mink, A.M. Vredenberg, F.H.P.M. Habraken, J. Appl. Phys. 105 (2009) 074305.
[16] K. Awazu, X. Wang, M. Fujimaki, J. Tominaga, H. Aiba, Y. Ohki, T. Komatsubara, Phys. Rev. B 78 (2008) 054102.
[17] K. Awazu, X. Wang, M. Fujimaki, J. Tominaga, S. Fujii, H. Aiba, Y. Ohki, T. Komatsubara, Nucl. Instrum. Methods B 276 (2009) 941.
[18] P. Kluth, R. Giulian, D.J. Sprouster, C.S. Schnohr, A.P. Byrne, D.J. Cookson, M.C. Ridgway, Appl. Phys. Lett. 94 (2009) 113107.
[19] In: Handbook of Nanostructured Materials and Nanotechnology, vol. 4, Academic Press, San Diego, 2000.
[20] A. Meldrum, L.A. Boatner, C.W. White, Nucl. Instrum. Methods B 178 (2001) 7.
[21] K. Awazu, C. Rockstuhl, M. Fujimaki, N. Fukuda, J. Tominaga, T. Komatsubara, T. Ikeda, Y. Ohki, Opt. Express 15 (2007) 2592.
[22] J.J. Penninkhof, Tunable Plasmon Resonances in Anisotropic Metal Nanostructures, Ph. D. Thesis, Utrecht University, 2006.
[23] A.I. Ryazanov, A.E. Volkov, S. Klaumünzer, Phys. Rev. B 51 (1995) 12107.
[24] F. Desauer, Z. Phys. 38 (1923) 12.
[25] F. Seitz, J.S. Koehler, Sol. State Phys. 2 (1956) 305.
[26] M. Toulemonde, C. Dufour, E. Paumier, Phys. Rev. B 46 (1992) 14362.
[27] R.L. Fleischer, P.B. Price, R.M. Walker, J. Appl. Phys. 36 (1965) 3645.
[28] D. Lesueur, A. Dunlop, Radiat. Eff. Defects Solids 126 (1993) 163.
[29] E. Dartyge, P. Sigmund, Phys. Rev. B 32 (1985) 5429.
[30] E.M. Bringa, R.E. Johnson, Phys. Rev. Lett. 88 (2002) 165501.
[31] P. Baril, L.J. Lewis, S. Roorda, Eur. Phys. J. B 71 (2009) 27.
[32] H. Trinkaus, A.I. Ryazanov, Phys. Rev. Lett. 74 (1995) 5072.
[33] H. Trinkaus, Nucl. Instrum. Methods B 146 (2001) 204.
[34] S. Klaumünzer, Nucl. Instrum. Methods B 225 (2004) 136.
[35] S. Klaumünzer, Nucl. Instrum. Methods B 244 (2006) 1.
[36] C. D'Orleans, J.P. Stoquert, C. Estournès, C. Cerruti, J.J. Grob, J.L. Guille, F. Haas, D. Muller, M. Richard-Poulet, Phys. Rev. B 67 (2003) 220101, (R).
[37] J.F. Ziegler, J.P. Biersack, U. Littmark, in: The Stopping and Ranges of Ions in Matter, version 2003.20, Pergamon, New York, 1985.
[38] G. Rizza, E.A. Dawi, A.M. Vredenberg, I. Monnet, Appl. Phys. Lett. 95 (2009) 043105.
[39] C. Riedel, R. Spohr, Radiat. Eff. 42 (1979) 69.
[40] C. Riedel, R. Spohr, Nucl. Tracks 5 (1981) 265.
[41] P. Kluth, C.S. Schnohr, O.H. Pakarinen, F. Djurabekova, D.J. Sprouster, R. Giulian, M.C. Ridgway, A.P. Byrne, C. Trautmann, D.J. Cookson, K. Nordlund, M. Toulemonde, Phys. Rev. Lett. 101 (2008) 175503.
[42] K. Awazu, S. Ishii, K. Shima, S. Roorda, J.L. Brebner, Phys. Rev. B 62 (2000) 3689.
[43] M.C. Ridgway, P. Kluth, R. Giulian, D.J. Sprouster, L.L. Araujo, C.S. Schnohr, D.J. Llewellyn, A.P. Byrne, G.J. Foran, D.J. Cookson, Nucl. Instrum. Methods B 276 (2009) 931.
[44] J. Jensen, A. Razpet, M. Skupinski, G. Possnert, Nucl. Instrum. Methods B 243 (2006) 119.
[45] N. Ishikawa Amekura, N. Okubo, M.C. Ridgway, R. Giulian, K. Mitsuishi, Y. Nakayama, Ch. Buchal, S. Mantl, N. Kishimoto, Phys. Rev. B 83 (2011) 205401.
[46] T. van Dillen, E. Snoeks, W. Fukarek, C.M. van Kats, K.P. Velikov, A. van Blaaderen, A. Polman, Nucl. Instrum. Methods B 175–177 (2001) 350.
[47] Ch. Dufour, V. Khomenkov, G. Rizza, M. Toulemonde, J. Phys. D: Appl. Phys. 45 (2012) 065302.